UC San Diego
International Symposium on Stratified Flows

Title

The effect of vortex pairing and Prandtl number on mixing in moderate Reynolds number stratified flows

Permalink

Journal

Authors

Dong, Wenjing
Rahmani, Mona
Lawrence, Gregory

Publication Date

2016-08-30

The effect of vortex pairing and Prandtl number on mixing in moderate Reynolds number stratified flows

Wenjing Dong[1], <u>Presenting Author</u>, Mona Rahmani[2], and Greg Lawrence[3]

[1]Department of Civil Engineering, University of British Columbia

wenjingdong11@hotmail.com

[2]Department of Mathematics, University of British Columbia

[3]Department of Civil Engineering, University of British Columbia

Abstract

Mixing resulting from Kelvin-Helmholtz instability is studied by direct numerical simulations for an intermediate Reynolds number in stratified flows where vortex pairing occurs. We investigate how the interaction of several billows changes the mixing properties. Simulations in a long domain show that only considering the interaction of two billows overestimates the amount of mixing and mixing efficiency. We also show that mixing is inhibited in high Prandtl number flows.

1. Introduction

Stratified flows are prevalent in nature. In this environment, Kelvin-Helmholtz (KH) instabilities may occur due to shear and cause mixing. KH instabilities begin with rolling up of the interface and then form elliptical billows (Corcos & Sherman (1976)) with finite amplitude. With the increasing turbulent motion, ensued from the growth of secondary instabilities, KH billows break down. Finally, turbulent motion is dissipated by viscous effects and the flow become laminar again. This whole process ends up with expanded velocity and density interfaces. During this process, the formation of large scale billows and breakdown of turbulent motions are main causes of mixing.

The amount of mixing due to Kelvin-Helmholtz (KH) instabilities in stratified flows can be characterized by the Reynolds number, the bulk Richardson number, and the Prandtl number. While there have been many studies of mixing in KH instabilities, most of them (e.g. Caulfield & Peltier (2000), Smyth, Moum, & Cardwell (2001), and Salehipour & Peltier (2015)) focus on Reynolds numbers above the mixing transition. However, in some circumstances, such as the internal seiche induced KH instabilities in lakes (Spigel & Imberger (1980)), low to intermediate Reynolds flows are expected that fall in the transitional range for mixing.

In this paper, we study KH instabilities for Reynolds number $Re = 1200$, and bulk Richardson number $J = 0.07$, in which vortex pairing occurs (Winant & Browand (1974)). To simulate a more realistic representation of shear instabilities in natural flows we extend our stream-wise length of the domain to11 most unstable wavelengths, calculated from linear stability analysis. We compare the results to the case when only two wavelengths are considered. The objective is to study how the interaction of several

billows in a long domain influences mixing. We also examine the effects of Prandtl number on mixing for each case.

2. Numerical model

We consider hyperbolic tangent initial background velocity profiles and density profiles

$$\bar{\rho} = \rho_0 - \frac{\Delta \rho}{2} \tanh\left(\frac{2z}{\delta_0}\right) \text{ and } \bar{U} = \frac{\Delta U}{2} \tanh\left(\frac{2z}{h_0}\right), \tag{1}$$

where h_0 is the thickness of velocity profile, δ_0 is the thickness of density profile, and ρ_0 is the reference density.

Assuming incompressible fluid and using the Boussinessq approximation, the governing equations of this flow are

$$\frac{D\boldsymbol{u}}{Dt} = -\frac{1}{\rho_0}\nabla p - \frac{\rho}{\rho_0}g\boldsymbol{k} + \nu\nabla^2\boldsymbol{u}, \tag{2}$$

$$\frac{D\rho}{Dt} = \kappa\nabla^2\rho. \tag{3}$$

The four important non-dimensional parameters in this flow are the bulk Richardson number, the Reynolds number, the Prandtl number, and the scale ratio which are defined respectively as

$$J = \frac{\Delta\rho g h_0}{\rho_0(\Delta U)^2}, \ \ Re = \frac{\Delta U h_0}{\nu}, \ \ \Pr = \frac{\nu}{\kappa}, \ \ R = \frac{h_0}{\delta_0}. \tag{4}$$

We fix J to 0.07 to study flow with moderate stratification, $Re = 1200$ and $R = 1$ in all simulations. For this combination of J and R, the Holmboe instability does not appear.

The governing equations are solved by a pseudo-spectral method with a third order time stepping scheme described in Winters, MacKinnon, & Mills (2004) and improved by Smyth, Nash, & Moum (2005). In this method, the grid spacing of density field is twice of the velocity field. To ensure enough resolution, grid spacing is less than 2.6 times of Batchelor length scale in all our simulations.

To initiate instability, but not favouring any modes, we add a random velocity noise to the background velocity. The magnitude of random noise is $0.1\Delta U$ with the maximum value located at the center of velocity profile. We apply periodic horizontal and free-slip vertical boundary conditions. $Lz = 15h_0$ is used to avoid boundary effects. The span-wise width Ly is one wavelength, and the length of the domain is either 2 wavelengths or 11 wavelengths of the predicted fastest growing instability.

3. Energy partition

To study the evolution of the flow, we analyze the energy budget following the work in Winters, Lombard, & Riley (1995). All the energy partitions are volume averaged and non-dimensionalized by $\rho_0(\Delta U)^2$. Time is non-dimensionlized by $h_0/\Delta U$ and energy transfer rates are non-dimensionalized by $\rho_0(\Delta U)^3/h_0$.

The non-dimensional kinetic energy is

$$K = \frac{\langle \boldsymbol{u} \cdot \boldsymbol{u} \rangle_{\mathrm{v}}}{2(\Delta U)^2}, \tag{5}$$

where v denotes a volume average.

It is divided into three components defined as (Caulfield & Peltier (2000))

$$K_{2d} = \frac{\langle \boldsymbol{u}_{2d} \cdot \boldsymbol{u}_{2d} \rangle_{xz}}{2(\Delta U)^2}, \; K_{3d} = \frac{\langle \boldsymbol{u}_{3d} \cdot \boldsymbol{u}_{3d} \rangle_{xyz}}{2(\Delta U)^2}, \; \text{and} \; \overline{K} = \frac{\langle \overline{\boldsymbol{u}} \cdot \overline{\boldsymbol{u}} \rangle_z}{2(\Delta U)^2}, \tag{6}$$

in which the subscript means average along that direction.

The non-dimensional potential energy is

$$P = \frac{g \langle \rho z \rangle_v}{\rho_0 (\Delta U)^2}. \tag{7}$$

It consists of background potential energy and available potential energy,

$$P_b = \frac{g \langle \rho z^* \rangle_v}{\rho_0 (\Delta U)^2}, \; P_a = P - P_b, \tag{8}$$

in which, z^* is the location of fluid parcels that are adiabatically rearranged into a statically stable profile as in Caulfield & Pieter (2000). The change of background potential energy results from irreversible mixing and molecular diffusion in a closed system. While, available potential energy reflects the energy that can be exchanged between potential energy and kinetic energy.

The time evolution of kinetic energy is determined by

$$\frac{dK}{dt} = -\psi - \varepsilon, \tag{9}$$

in which, ψ is buoyancy flux and ϵ is viscous dissipation rate defined as

$$\varepsilon = \frac{h_0}{\rho_0 (\Delta U)^3} \langle 2\mu S_{ij} S_{ij} \rangle_v, \tag{10}$$

in which S is strain tensor. The time evolution of potential energy is controlled by

$$\frac{dP}{dt} = \psi + \phi_i, \tag{11}$$

in which, ϕ_i is molecular diffusion defined as

$$\phi_i = \frac{h_0}{\rho_0 (\Delta U)^3} \frac{-\kappa g (\bar{\rho}_{top} - \bar{\rho}_{bottom})}{L_z}. \tag{12}$$

The amount of mixing is the increase of background potential energy minus the increase from molecular diffusion ϕ_i, i.e.

$$M = \Delta P_b - \phi_i t = \int \phi_M dt, \tag{13}$$

where ϕ_M is the rate of mixing. To reflect how much energy is used to mix, mixing efficiency is defined as the ratio of energy used to mix and the energy that is irreversibly lost (Caulfield & Peltier (2000)), i.e.

$$E_i = \frac{\phi_M}{\phi_M + \varepsilon}. \tag{14}$$

This mixing efficiency is a function of time. To reflect the mixing efficiency in a period, cumulative mixing efficiency is introduced, which is defined as (Caulfield & Peltier (2000))

$$E_c = \frac{\int \phi_M dt}{\int \phi_M dt + \int \varepsilon dt} \tag{15}$$

4. Results

4.1. The effects of interaction of several billows

We divide the life cycle of KH instabilities into 3 stages. During the first stage, billows grow and pair. The first local maximum of potential energy marks the end of this stage. We use t_1 to denote this time. During the second stage, turbulent motion becomes important. We use t_2 to denote the time when K_{3d} reaches its maximum as the end of this stage. During the final stage, turbulence decays. We define t_3 as the time when K_{3d}/K_0 first drops to 10^{-3} to mark the end of this stage, in which K_0 is the initial kinetic energy. Figure 1 shows snapshots of the evolution of several billows at first two transition times and when maximum potential energy is reached, where the initial length of the domain has been set to 11 wavelengths of the fastest growing instability. At t_1, the number of billows has reduced to 7 due to vortex pairing. Each billow follows a different pairing style because of the randomness of the perturbation of the velocity field. However, not all billows merge before the growth of secondary instabilities, suggesting that mixing in a series of many billows can be significantly different from the case of two merging billows. At t_2, when three-dimensionality is strongest, the billows at the boundary are still merging and less susceptible to secondary instabilities than other billows.
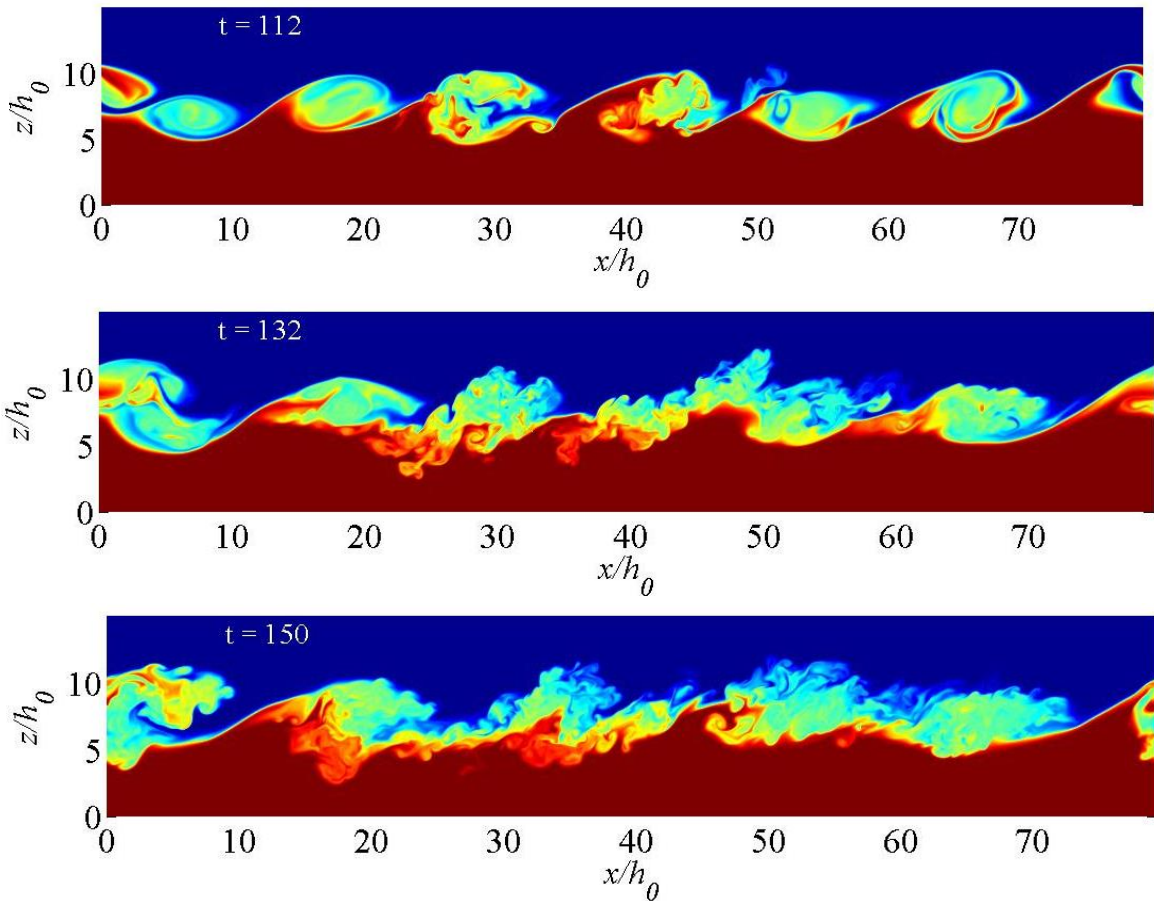

Figure 1: Snapshots of stream-wise density field at $y = L_y/2$ at first local maximum of potential energy, maximum of three dimensional turbulent kinetic energy, and maximum of potential energy. For this simulation, $Re = 1200$, $Pr = 1$, and $J = 0.07$.

In figure 2 we compare the evolution of the energy partitions for domains with stream-wise length of 11 and 2 wavelengths. During the primary KH billow growth, P increases more quickly in the 2 wavelengths simulation indicating faster billow growth. As shown in figure 1, at the first local peak of P some billows have merged, while merging has been supressed by the growth of secondary instabilities for other billows. The development of three-dimensional motions through the flow for the 11 wavelength simulation is reflected by the non-negligible K_{3d} at t_1. At this time the stirring is significantly lower for the11 wavelength simulation, but the amount of mixing is similar. In the next stage, a relatively large part of potential energy is transferred to K_{3d} by turbulent buoyancy flux, which is achieved by the oscillation of the large billow in the 2 wavelengths simulation. However, in the 11 wavelengths simulation, potential energy experiences a short intermittency and then rises. The reason is that pairing proceeds at different rates in different parts of the domain, see figure1.

In the next stage, potential energy rises until it reaches its second peak (also the maximum) when pairing is completely finished for the 11 wavelength simulation (see the last panel in figure 1). After this second peak of potential energy, large scale motions are destroyed and then the flow enters its real turbulent decay stage. At the end of the life cycle, the amount of mixing is slightly lower for the 11 wavelengths. So the 2 wavelengths simulation tends to overestimate mixing because of the earlier merging process of billows.
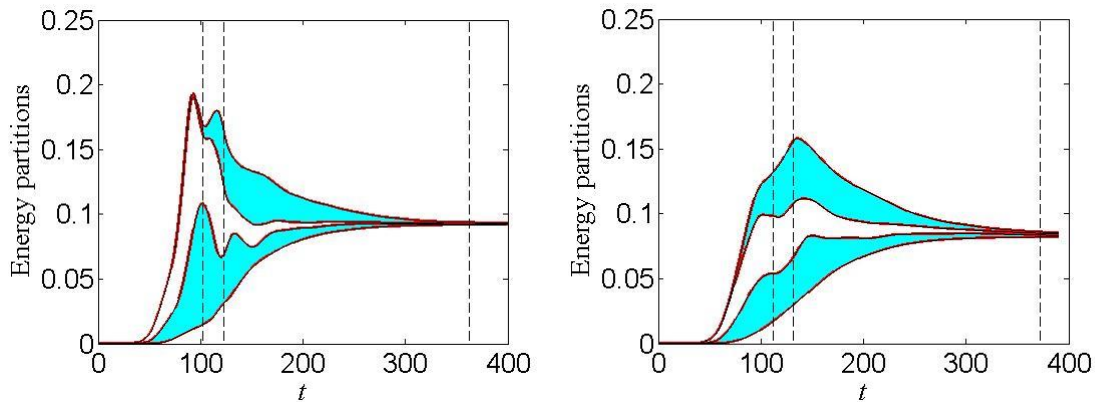

Figure 2: Evolution of energy partitions which are normalized by K_0. The left is the 2 wavelengths simulation. The right is the 11 wavelengths simulation. From bottom to top, fours lines are respectively P_b, P, $P + K_{2d}$, and $P + K_{2d} + K_{3d}$, and the blue shadings are respectively P_a and K_{3d}. The vertical lines show the transition times.

In figure 3, we plot the instantaneous mixing efficiency E_i in 2 wavelengths simulation and 11 wavelengths simulation. Overall, two simulations have similar pattern of E_i. The maximum E_i is higher in the 2 wavelengths simulation because billows pair more effectively before strong turbulence develops. During the turbulent decay stage, two simulations have same mixing rate. This is because turbulence is quite uniform over the domain.

The lower instantaneous mixing efficiency in the 11 wavelengths simulation results in a lower cumulative mixing efficiency at the end of the life cycle ($E_c = 0.265$) than in the 2 wavelengths simulation ($E_c = 0.307$). The latter is a little lower than the value in 2 wavelength simulation in Smyth, Moum, &

Cardwell (2001). We speculate this is because we do not perturb the velocity using the most unstable mode. The cumulative mixing efficiency in the 11 wavelengths simulation is higher than values in the single wavelength simulations of Rahmani, Seymour, & Lawrence (2016) and Salhipour & Peltier (2015).
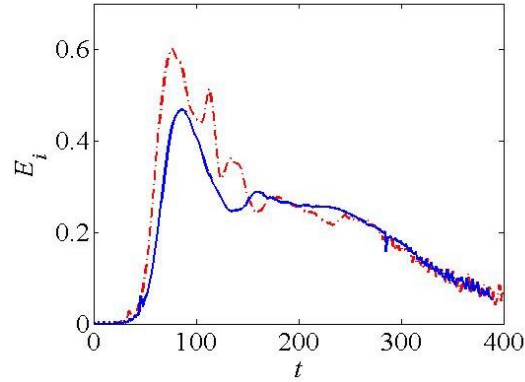

Figure 3: E_i in the 2 wavelengths simulation (red dash-dotted line) and the 11 wavelengths simulation (blue solid line).

4.2. The effects of Prandtl number

While work is still in progress to investigate the effects of Prandtl number on the interactions of several billows, we have examined the effects of Prandtl number for 2 wavelength simulations. Figure 4 shows the density field of the flow for 2 wavelength simulations at $Pr = 1$, 9 and 16. Finer scale structures appear in the flow as Pr increases.
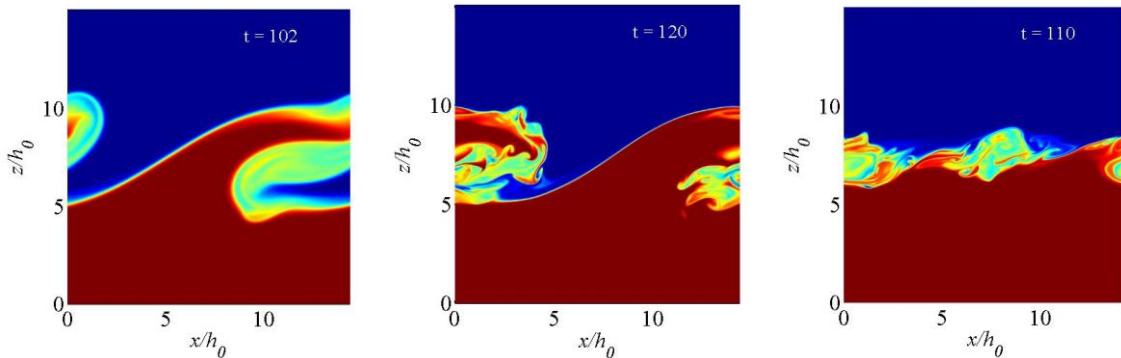

Figure 4: The first two are density field at first local maximum of potential energy for $Pr = 1$ and 9. The third one shows that no pairing occurs for $Pr = 16$.

In figure 5, we plot the energy partitions for $Pr = 1$, 9, and 16. When Pr increases from 1 to 9, the first peak of potential energy decreases due to earlier development of small scale motions which are shown in figure 4. At $Pr = 16$, the two billows are destroyed by small scale motions before pairing (see figure 4). So the first peak occurs earlier. Due to the decreasing diffusivity, the amount of mixing also decreases as Pr increases. At the end of KH instabilities, the amount of energy that is extracted from mean kinetic energy to final potential energy is significantly suppressed at high Pr. This is different from the case of high Reynolds number in Salehipour & Peltier (2015).
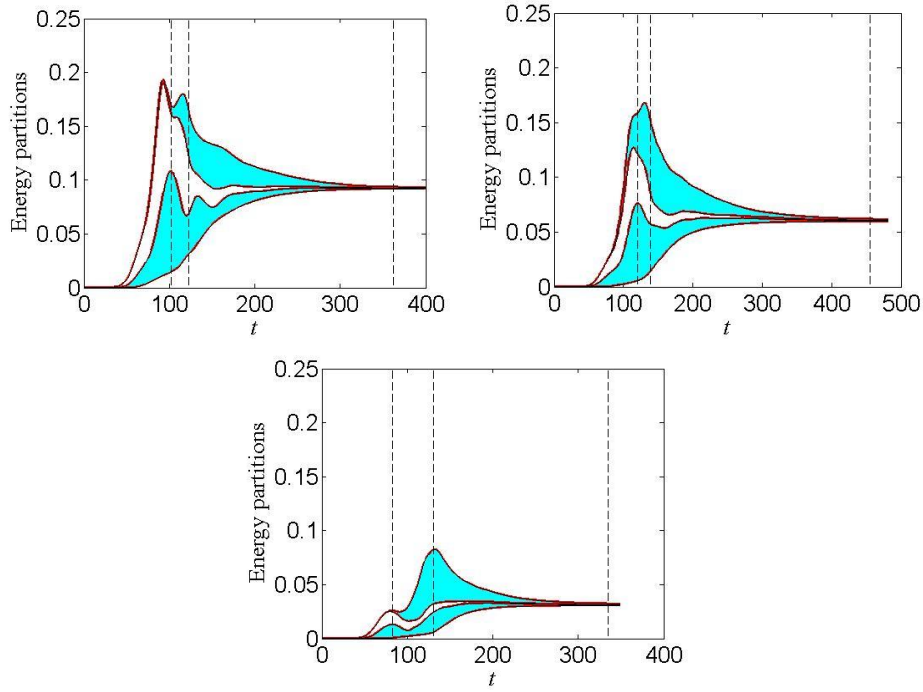
Figure 5: Evolution of energy partitions. From bottom to top, fours lines are respectively P_b, P, $P + K_{2d}$, and $P + K_{2d} + K_{3d}$, and the blue shadings are respectively P_a and K_{3d}. The vertical lines show the transition times defined in section 4.1. From the first to the last, $Pr = 1$, 9, and 16.

Instantaneous mixing efficiency of $Pr = 1$, 9, and 16 is plotted in figure 6. When Pr increase from 1 to 9, the mixing efficiency significantly shrinks due to the slower molecular diffusion. As Pr increase from 9 to 16, the mixing efficiency decreases less, because the change of diffusivity is relatively small.
The first peak of E_i is associated with the growing billows. At the maximum point, turbulence is not very strong and molecular diffusion is dominant. So the first peak of $Pr = 1$ is much higher than those for other case. When turbulent mixing becomes important, the mixing efficiency exhibits more similar values for all cases. The final cumulative mixing efficiencies are respectively 0.307, 0.184, and 0.143 for $Pr = 1$, 9, and 16. This decreasing trend is consistent with Smyth, Moum, & Cardwell (2001), Salhipour & Peltier (2015), and Rahmani, Seymour, & Lawrence (2016).
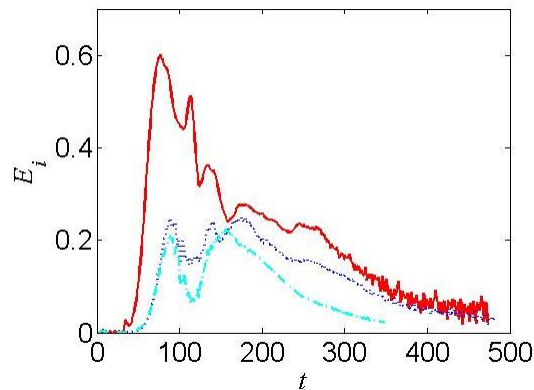

Figure 6: Mixing efficiency as $Pr = 1$ (red solid line), 9 (blue dotted line), and 16 (cyan dash-dotted line).

5. Conclusions

The evolution of energy partitions and mixing in stratified flows that differ only in Pr or domain length have been compared. When Pr increases from 1 to 9, the destruction of pairing happens earlier but the vertical extent of large scale motion is comparable. The amount of mixing decreases about by one-half due to the slower molecular diffusion. When Pr increases from 9 to 16, two billows are destructed by three dimensional motions before pairing occurs. This lower extent of vertical motions decreases the amount of mixing further, in addition to smaller diffusivity.

Another conclusion is that the two wavelengths simulation tends to maximize pairing and overestimate the amount of mixing. In multiple wavelengths domain, the pairing process is quite random and the average amount of mixing is lower. While the amount of mixing is less in a domain of multiple wavelengths than one of two wavelengths, it is more than for a single wavelength domain.

References

Corcos, G. M., & Sherman, F. S. (1976). Vorticity concentration and the dynamics of unstable free shear layers. *Journal of Fluid Mechanics*, *73*(02), 241-264.

Caulfield, C. P., & Peltier, W. R. (2000). The anatomy of the mixing transition in homogeneous and stratified free shear layers. *Journal of Fluid Mechanics*,*413*, 1-47.

Smyth, W. D., Moum, J. N., & Caldwell, D. R. (2001). The efficiency of mixing in turbulent patches: Inferences from direct simulations and microstructure observations. *Journal of Physical Oceanography*, *31*(8), 1969-1992.

Salehipour, H., & Peltier, W. R. (2015). Diapycnal diffusivity, turbulent Prandtl number and mixing efficiency in Boussinesq stratified turbulence. *Journal of Fluid Mechanics*, *775*, 464-500.

Winant, C. D., & Browand, F. K. (1974). Vortex pairing- The mechanism of turbulent mixing-layer growth at moderate Reynolds number. *Journal of Fluid Mechanics*, *63*(2), 237-255.

Winters, K. B., MacKinnon, J. A., & Mills, B. (2004). A spectral model for process studies of rotating, density-stratified flows. *Journal of Atmospheric and Oceanic Technology*, *21*(1), 69-94.

Smyth, W. D., Nash, J. D., & Moum, J. N. (2005). Differential diffusion in breaking Kelvin-Helmholtz billows. *Journal of physical oceanography*, *35*(6), 1004-1022.

Winters, K. B., Lombard, P. N., Riley, J. J., & D'Asaro, E. A. (1995). Available potential energy and mixing in density-stratified fluids. *Journal of Fluid Mechanics*, *289*, 115-128.

Rahmani, M., Seymour, B. R., & Lawrence, G. A. (2016). The effect of Prandtl number on mixing in low Reynolds number Kelvin-Helmholtz billows.*Physics of Fluids*, *28*(5), 054107.